

# Measuring Single-Walled Carbon Nanotube Length Distributions from Diffusional Trajectories

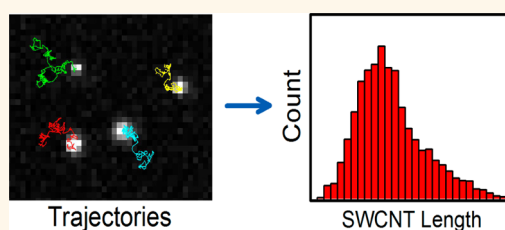
Jason K. Streit,<sup>†</sup> Sergei M. Bachilo,<sup>†</sup> Anton V. Naumov,<sup>†,‡</sup> Constantine Khripin,<sup>§</sup> Ming Zheng,<sup>§</sup> and R. Bruce Weisman<sup>†,\*</sup>

<sup>†</sup>Department of Chemistry and Richard E. Smalley Institute for Nanoscale Science and Technology, Rice University, 6100 Main Street, Houston, Texas 77005, United States, <sup>‡</sup>Ensysce Biosciences, Inc., 7000 Fannin Street, Houston, Texas 77030, United States, and <sup>§</sup>Polymers Division, National Institute of Standards and Technology, 100 Bureau Drive, Gaithersburg, Maryland 20899, United States

The lengths of single-walled carbon nanotubes (SWCNTs) may vary by orders of magnitude, from a few tens of nanometers up to several centimeters, through variations in growth conditions and subsequent processing. These differences can have important consequences, as nanotube length is a relevant parameter for a variety of fundamental processes and applications. For example, it has been reported that cellular uptake of DNA-wrapped SWCNTs favors lengths of ~200 to 300 nm.<sup>1,2</sup> This implies that nanotube length should be monitored and controlled to optimize many drug delivery and bioimaging applications. Length is also important in the performance of single-nanotube electronic devices and in determining the density of nanotubes needed to form conductive networks.<sup>3,4</sup> In using nanotubes for mechanical strengthening of composite materials, load transfer efficiency is also dependent on nanotube lengths.<sup>5,6</sup> The development of methods to tailor length distributions through controlled growth or postgrowth fractionation clearly requires the use of practical and efficient analytical methods that reveal length values.

The standard current method for measuring SWCNT lengths is through analysis of atomic force microscopy (AFM) images.<sup>7,8</sup> Although widely used, this technique requires careful sample preparation followed by relatively time-consuming data acquisition. Skilled manual analysis of the resulting image to obtain a length histogram is tedious if a large enough sample is measured to give good statistics, but the process can often be automated through the use of specialized software designed to recognize individual nanotubes, compute their apparent lengths from the image, and compile a

## ABSTRACT



A new method is demonstrated for measuring the length distributions of dispersed single-walled carbon nanotube (SWCNT) samples by analyzing diffusional motions of many individual nanotubes in parallel. In this method, termed “length analysis by nanotube diffusion” (LAND), video sequences of near-IR fluorescence microscope images showing many semiconducting SWCNTs are recorded and processed by custom image analysis software. This processing locates the individual nanotubes, tracks their translational trajectories, computes the corresponding diffusion coefficients, and converts those values to nanotube lengths. The deduced length values are then compiled into a histogram of lengths present in the sample. By using specific excitation wavelengths and emission filters, this analysis is performed on selected  $(n,m)$  structural species. The new LAND method has been found to give distributions in very good agreement with those obtained by conventional AFM analysis of the same samples. Because it is fluorescence-based, LAND monitors only semiconducting, relatively pristine SWCNTs. However, it is less sensitive to artifacts from impurities and bundled nanotubes than AFM or light scattering methods. In addition, samples can be analyzed with less time and operator attention than by AFM. LAND is a promising alternative method for characterizing length distributions of SWCNTs in liquid suspension.

**KEYWORDS:** SWCNT · single-walled carbon nanotubes · single-particle tracking · length · fluorescence · diffusion

histogram of the results. AFM findings can be compromised by the presence of nanotube aggregates and impurities unless they are distinguished from individual SWCNTs by height measurements.

Depolarized dynamic light scattering<sup>9,10</sup> (DDLS) and multiangle light scattering (MALS)<sup>11–13</sup> are the most commonly used bulk methods for characterizing lengths of SWCNT samples in liquid suspensions.

\* Address correspondence to weisman@rice.edu.

Received for review July 20, 2012 and accepted August 27, 2012.

Published online August 27, 2012  
10.1021/nn3032744

© 2012 American Chemical Society

However, they are most accurate for relatively mono-disperse samples and can reliably provide only average lengths rather than full length distributions. The effectiveness of light scattering methods can be limited by sensitivity to artifacts from nanotube aggregates or impurities in the sample.

Casey *et al.* developed a bulk method for SWCNT characterization based on the length-dependent alignment of nanotubes suspended in liquids undergoing shear flow.<sup>14</sup> In this method, nanotube alignment is measured using near-IR fluorescence spectroscopy with polarized light, exploiting the highly anisotropic optical transitions of SWCNTs. The sample's length distribution is deduced from the extent of alignment measured as a function of shear. Because it is spectroscopically based, this method provides  $(n,m)$ -resolved length information for semiconducting SWCNTs and is insensitive to impurities and most bundled nanotubes. However, the rapid rotational diffusion of shorter nanotubes prevented the alignment and resolution of SWCNTs with lengths below  $\sim 500$  nm at accessible shear levels.

Recently our laboratory has shown that the length of a SWCNT can be deduced from near-IR fluorescence microscope image sequences that show its translational diffusion in a liquid environment.<sup>15,16</sup> This approach exploits the remarkable stability of SWCNT fluorescence,<sup>17–19</sup> which is generally free of the photobleaching and intermittency that can make individual organic fluorophores or quantum dots difficult to track. In our method, the Brownian motion of an individual nanotube is quantitatively analyzed to find its translational diffusion coefficient. A simple relation then gives that nanotube's length from the diffusion coefficient. Although this fluorescence-based method cannot observe metallic SWCNTs, it can spectroscopically select particular semiconducting  $(n,m)$  species and it is immune to interference from impurities or most nanotube bundles (which are generally non-emissive). In a recent study using a similar approach, Strano and co-workers tracked diffusional trajectories of individual SWCNTs to probe viscosities inside living cells.<sup>20</sup> We report here an important extension of diffusional tracking to accurately capture, analyze, and deduce lengths for dozens of nanotube trajectories in parallel. This large enhancement in efficiency introduces a practical new way to measure statistically valid length distributions of SWCNT samples in fluid suspension, with some benefits as compared to AFM analysis. We term the new method LAND (length analysis from nanotube diffusion).

## ANALYSIS METHOD

As described in detail in the Experimental Methods section, we used a customized microscope to capture wide-field near-IR fluorescence images of surfactant-coated SWCNTs as they diffused freely in aqueous

suspension. Samples were typically contained in microwells that had been wet-etched into a glass microscope slide. These wells were etched to a depth that matched the optical depth of field of our microscope objective, ensuring that all SWCNTs remained in focus throughout the 1001 sequential frames of each video data set. We wrote custom image analysis software, using Matlab 2011a (Mathworks), to locate all SWCNTs in the image field and track their translational motions. In brief, the software begins by identifying and determining the centroid position of each nanotube in the field to a precision of 50 nm. Single nanotube trajectories are created using a nearest-neighbor algorithm that connects positions in consecutive images. However, it may happen that a nanotube is not visible in the following frame. One reason for this is that SWCNT images exhibit fluorescence intensity modulation due to out-of-plane rotational motion, even with circularly polarized excitation.<sup>16</sup> If an identified nanotube is lost in the next frame, then the search window is widened. If it has not reappeared within five frames, then its trajectory is automatically terminated. Another complication is that two SWCNTs may diffuse so close to each other that their images cannot be distinguished. When this occurs, both trajectories are terminated. To minimize trajectory fragmentation from such particle overlap, nanotube densities are kept below  $\sim 70$  SWCNTs/image. Our algorithm proceeds to evaluate the spatial, temporal, and intensity parameters of the interrupted trajectory fragments to help identify fragments that correspond to the same nanotube and to combine them into a single trajectory if they match. Nevertheless, we find that many trajectories will typically remain fragmented.

Each nanotube trajectory is numerically analyzed by calculating  $\langle \mathbf{r}^2 \rangle$ , the mean-square displacement (MSD), as a function of frame count  $n$  using the standard formula:<sup>21,22</sup>

$$\langle \mathbf{r}^2 \rangle_n = \frac{1}{N-n} \sum_{i=1}^{N-n} (\mathbf{r}_{i+n} - \mathbf{r}_i)^2$$

$$n = 1, \dots, N-1 \quad (1)$$

Here  $N$  is the total number of frames (1001) and  $\mathbf{r}$  is the particle position vector. Linear behavior in a plot of  $\langle \mathbf{r}^2 \rangle$  vs lag time (or  $n\delta t$ , where  $\delta t$  is the frame interval) indicates simple diffusive motion, and the translational diffusion coefficient is then proportional to the slope. However, when computing the MSD it is important to address the experimental influence of localization uncertainty in single-particle tracking experiments. Localization uncertainty has static and dynamic components. The static uncertainty is defined as the standard deviation of an immobilized particle's apparent position and is inversely proportional to the square root of the brightness of that particle's image.<sup>23,24</sup> Dynamic localization uncertainty arises from motion blur caused

by particle movement during the exposure time.<sup>25,26</sup> Including these sources of uncertainty, the MSD for a two-dimensional diffusional trajectory is expressed as<sup>25–28</sup>

$$\text{MSD} = 4D_{\text{TR}}t + 4\sigma^2 - \frac{4}{3}D_{\text{TR}}t_{\text{E}} \quad (2)$$

where  $D_{\text{TR}}$  is the translational diffusion coefficient,  $t$  is lag time,  $\sigma$  is the static localization uncertainty, and  $t_{\text{E}}$  is the exposure time. Dynamic localization uncertainty gives the last term of  $-\frac{4}{3}D_{\text{TR}}t_{\text{E}}$  in eq 2. Although SWCNTs are diffusing in three-dimensional space, we observe only a two-dimensional projection of their Brownian motion, requiring use of the two-dimensional equation shown above. A plot of MSD vs lag time is constructed for every nanotube trajectory and a two-point linear fit is applied to each, where the slope and intercept are

$$\text{slope} = 4D_{\text{TR}} \quad (3)$$

$$\text{intercept} = 4\sigma^2 - \frac{4}{3}D_{\text{TR}}t_{\text{E}} \quad (4)$$

Calculation of the mean-square displacement has been widely used for many years as a tool to study the diffusion of small particles and molecules, but systematic studies on optimizing translational diffusional analyses in the presence of experimental uncertainties have only recently been reported.<sup>27,28</sup> To better understand such effects, we used a two-dimensional random walk algorithm to simulate the Brownian motion of particles with a fixed value of  $D_{\text{TR}}$ . Variable amounts of relative experimental uncertainty,  $X = (\sigma^2/(D_{\text{TR}}\delta_t))$ ,<sup>27</sup> were added to each simulated random walk with 1001 steps, and 100 000 trajectories were simulated for each uncertainty value. Then, for each of these synthetic trajectories, we found the slope between the first and the  $n$ th points on the MSD vs lag time plot and calculated the relative standard deviation of those slopes as a function of uncertainty  $X$  and the integer  $n$ . (Standard deviations will also depend on number of steps in each trajectory.) These results are plotted in Figure 1a. The minimum in each curve indicates the second point on an MSD plot that should be used to obtain the most reliable estimate of slope and thus diffusion coefficient. In agreement with the report by Michalet,<sup>27</sup> we find that the optimal second point index changes from approximately 2 to 6 as the experimental uncertainty  $X$  increases from 0 to 5. The smooth curves shown in Figure 1a were constructed using functions described in the Supporting Information.

To apply these findings to experimental data, we need to estimate the value of  $X$  for each measured trajectory. We begin by using the first two MSD points to obtain a slope approximating  $4D_{\text{TR}}$  (eq 3) and an intercept representing  $4\sigma^2 - \frac{4}{3}D_{\text{TR}}t_{\text{E}}$  (eq 4). These estimated values are then combined to give an approximate static localization uncertainty,  $\sigma$ . The

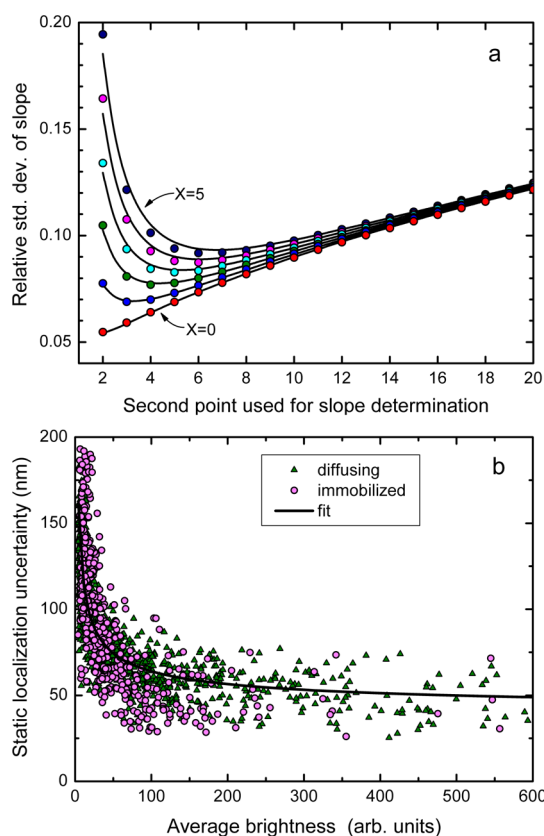


**Figure 1.** Parameters related to analysis of MSD data. (a) Standard deviations of the slopes found from synthetic MSD plots as a function of the index,  $n$ , of the second point used for determining the slope. Separate results are plotted for varying levels of positional uncertainty,  $X$ , as given in the text. Smooth curves show fits calculated according to expressions given in the Supporting Information. (b) Experimental static localization errors measured for SWCNTs that were diffusing (triangles) or immobilized (circles), as a function of their imaged brightness,  $I$ . The solid curve is a best fit of the form  $I^{-1/2}$ .

symbols in Figure 1b show these experimental localization uncertainties extracted from individual nanotube MSD curves plotted *versus* nanotube image brightness. The smooth curve in the figure shows the expected dependence of  $\sigma$  on the square root of brightness. An alternative method for determining  $\sigma$  is recording repeated images of immobilized SWCNTs and calculating the standard deviation of their apparent positions. Figure 1b shows that the static errors measured from immobilized nanotubes follow the same trend as those estimated from diffusing nanotubes. This indicates that under our current experimental conditions,  $\sigma$  can be reliably calculated from the slopes and intercepts of MSD curves. Once  $\sigma$  has been estimated, we use it to find the value of  $X$  to optimize the MSD slope determination and to estimate uncertainty in the deduced diffusion coefficient. We find that most experimental  $X$  values are below 3, with a few reaching values as high as 5. Average relative uncertainties in the diffusion coefficients are  $\sim 10\%$ .

After the diffusion coefficient has been estimated for each individual SWCNT, we proceed to calculate the nanotube length. Since SWCNTs shorter than  $\sim 3 \mu\text{m}$  can be considered rigid rods in fluid suspension,<sup>29,30</sup> the translational diffusion coefficient is expressed by the following relation from Aragon and Flamik:<sup>31</sup>

$$D_{\text{TR}} = \frac{k_{\text{B}}T}{\pi\eta_s} \frac{\ln(L/d) + X(L/d)}{L} \quad (5)$$

where  $k_{\text{B}}$  is the Boltzmann constant,  $T$  is the sample temperature (295 K),  $\eta_s$  is the effective solution viscosity,  $L$  is nanotube length,  $d$  (estimated to be  $5 \pm 2 \text{ nm}$ )<sup>15,16,32</sup> is the hydrodynamic diameter including the surfactant coating, and  $X$  represents the end correction coefficients, which have a complex dependence on aspect ratio. To account for wall-drag and related effects in thin liquid films, we take  $\eta_s$  to be 1.9 times the measured bulk viscosity.<sup>15,16</sup> Every full and partial nanotube trajectory is analyzed to deduce the corresponding length. However, to minimize uncertainties, we reject trajectories shorter than 100 frames or with uncertainties in diffusion coefficient above 25%. All deduced nanotube lengths are subsequently compiled to generate a histogram representing the sample's length distribution, but to avoid overcounting SWCNTs with fragmented apparent trajectories, the y-axis histogram values are weighted by the number of image frames in the corresponding trajectory. In this way, the two 500-frame trajectory fragments belonging to a single nanotube are given the same total weight as one uninterrupted 1000-frame trajectory.

## RESULTS AND DISCUSSION

To test the validity of the LAND technique, we recorded and analyzed 20 videos of an aqueous suspension enriched in (6,5) SWCNTs. The enrichment was achieved through nonlinear density-gradient ultracentrifugation.<sup>33</sup> To slow down SWCNT motion and to aid in particle tracking, solution viscosity was increased to 30 mPa-s (see Methods). Figure 2 shows a comparison of the length histograms measured by LAND and AFM. Since relatively large numbers of nanotubes were observed, it is appropriate to compare the statistics of the two distributions. The calculated mean and standard deviation of the lengths measured by LAND and AFM were found to be 427 and 267 nm, respectively, from LAND, as compared to 445 and 310 nm from AFM. These values differ between methods by 4% for the means and 14% for standard deviations. We view the agreement as very satisfactory. The two deduced distributions also have similar shapes, but there is a 52 nm (26%) difference between the peaks of their log-normal fits. In addition, we note that the LAND method successfully characterized the wide range of SWCNT lengths ( $\sim 50$ –1830 nm) present in this polydisperse sample. LAND resolved nanotubes as short as 50 nm, a lower limit that is comparable to

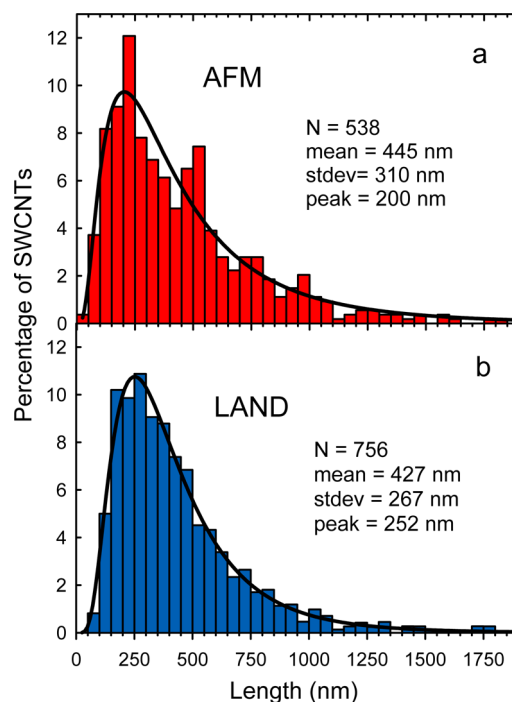


**Figure 2.** Comparison of length histograms found by (a) AFM and (b) LAND analyses of the same (6,5)-enriched SWCNT sample. Solid curves are log-normal fits ( $r^2 = 0.936$  for AFM and 0.988 for LAND) used to estimate the peak values listed in the frame. The other statistical parameters were computed from the histogram data rather than from the fits.

that of most AFM analyses. By acquiring LAND data at more than one sample viscosity, one can extend the range of analyzed nanotube lengths.

For the LAND method to accurately measure the full distribution of lengths in a SWCNT sample, nanotubes of all lengths must be reliably imaged. Since SWCNT fluorescence emission increases linearly with length,<sup>15</sup> there is concern that shorter nanotubes will appear too weak to be detected. If this is the case, then the length distribution measured by LAND will be falsely shifted to longer lengths. To study whether the histogram shown in Figure 2b might be distorted by limited sensitivity to SWCNT fluorescence, two additional sets of videos were acquired using lower excitation powers. Figure 3 compares the resulting distributions obtained at the three different excitation levels. As the power density was increased from 0.5 to 1.0  $\text{kW}/\text{cm}^2$ , the length distribution shifted to substantially shorter values, with the calculated mean length decreasing by  $\sim 26\%$  to  $\sim 430 \text{ nm}$ . This indicates that we failed to observe a significant percentage of the short SWCNTs under low power excitation. More evidence of this effect is found in the number of nanotubes detected, which rose from 20 to 38 per frame. However, as seen from Figure 3, a further increase in excitation intensity to 1.4  $\text{kW}/\text{cm}^2$  produced negligible change in the deduced length distribution. This implies adequate detection of SWCNTs within the relevant length range at the higher

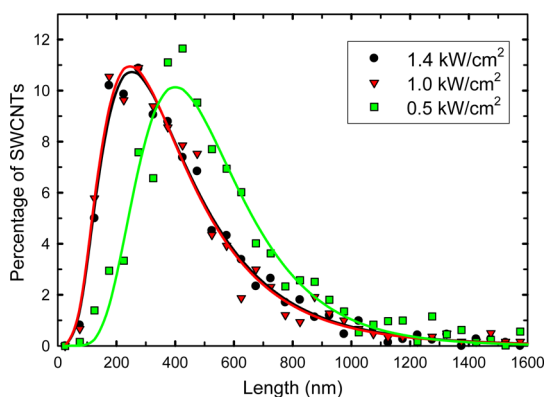


**Figure 3.** Length distribution of the same SWCNT sample deduced by LAND analysis with three different excitation intensities. Points are measured histogram data and solid curves show log-normal best fits.

excitation levels and also demonstrates the method's reproducibility. We conclude that distribution accuracy is dependent on experimental conditions and emissive properties of the SWCNT sample. LAND length measurements will be most accurate when higher excitation powers are used. Additionally, sample cells should be made from fused silica or high quality glass to reduce background fluorescence levels and improve image contrast. Careful consideration should also be given to the intrinsic brightness of the sample. Chemical functionalization or high defect concentrations will lower the quantum yield, increasing the likelihood that shorter nanotubes remain undetected.

To further demonstrate the capabilities of LAND, distributions were measured for two length-sorted samples of CoMoCAT SWCNTs. These fractions ( $F_n$ ) were prepared using a new method based on SWCNT clustering induced by molecular crowding (see Methods).<sup>34</sup> Although CoMoCAT samples contain several semiconducting ( $n,m$ ) species, not all of these can be conveniently excited on resonance. Shorter nanotubes or species excited off resonance will emit less intensely, decreasing the probability that they will be adequately imaged. Therefore, when working with ( $n,m$ )-polydisperse samples it is preferable to optically select for a single species using efficient on-resonance excitation and spectrally filtered imaging. Here we again chose to analyze the motions of (6,5) SWCNTs because of the high sensitivity already demonstrated for this species. Fraction 5 (F5) comprises shorter SWCNTs, as can be seen from the LAND and AFM length histograms compared in Figure 4a. The LAND method found a mean and standard deviation of 233 and 107 nm, in good agreement with the corresponding AFM values of 211 and 113 nm. Both measurements display a similar range of lengths, and the peak positions of the log-normal fits differ by only 1%, although some shape differences can be seen.

F8 contains a broader length distribution, as shown in Figure 4b. LAND deduced the average and standard

deviation of the distribution to be 609 and 240 nm, as compared to AFM values of 515 and 254 nm. Although the deviation in calculated means is  $\sim 18\%$ , the distribution shapes are fairly similar. Overall, we consider that the agreement between AFM and LAND results is satisfactory for both fractions.

It should also be noted that while our current LAND measurements find the lengths only of (6,5) SWCNTs, AFM measures all ( $n,m$ ) species, including metallic nanotubes, present in the two samples. Although we do not expect length distributions to differ for metallic and semiconducting SWCNTs in a given sample, some evidence has been reported for a positive correlation between average nanotube length and diameter in mildly sonicated dispersions.<sup>14</sup> In such cases, the results from our method may deviate from the length distribution of the entire sample. However, comparison of the AFM and LAND results in Figure 4, on samples containing a range of lengths and diameters and exposed to typical dispersion processing, does not suggest a positive correlation between nanotube length and diameter. Thus it seems likely that ( $n,m$ )-specific LAND results will adequately represent overall length distributions for most dispersed SWCNT samples.

It is important to consider possible sources of error that might limit the reliability of the LAND method. One is the statistical uncertainty in the diffusion coefficient of any particle when determined over a finite observation period. Such errors are greater for shorter nanotubes, because their dimmer images and rapid motions make them more difficult to track without interruption. In our experiments, their trajectories typically do not span the full 1001 frame video sequence. Additionally, experimental errors due to positional uncertainty and motion blur will be higher in the trajectories of short SWCNTs. The combination of these factors will increase errors in the diffusion coefficient and the deduced nanotube length. Also, uncertainty in hydrodynamic diameter may cause additional errors. We estimate that the combined uncertainties in diffusion coefficient and nanotube diameter can give relative length errors ranging from  $+20/-15\%$  for 50 nm long nanotubes to  $\pm 11\%$  for 2000 nm long nanotubes.

One type of systematic error involves convective motion of the observed particles. To check for such effects, we have computed the average net displacements (from initial to final image frames) along the  $x$ - and  $y$ -axes for all nanotubes detected in a video sequence. As graphed in Supporting Information, Figure S1, we find average drifts below 10 nm/s ( $\sim 1$  nm per 150 ms frame), varying randomly among video sequences. These values indicate that convection can be neglected relative to diffusion in our samples. Systematic errors might also arise from a length dependence in the wall-drag correction factor, which

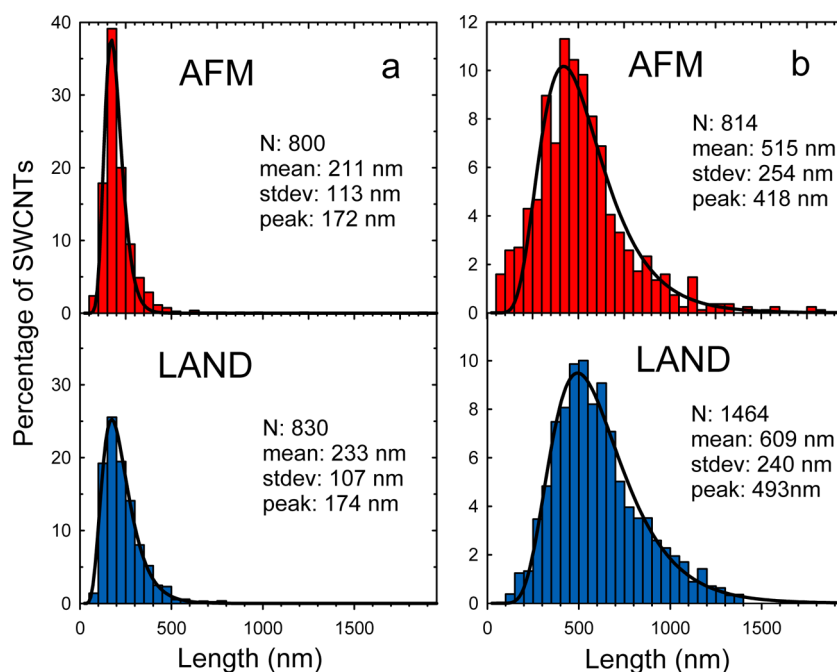


**Figure 4.** Comparison of length histograms found by AFM (top frames) and LAND (bottom frames) for two different length-sorted SWCNT fractions: (a) F5, (b) F8. Solid curves are log-normal fits ( $r^2 = 0.986$  for F5 AFM, 0.995 for F5 LAND, 0.940 for F8 AFM, and 0.985 for F8 LAND) used to estimate the peak values listed in the frame. The other statistical parameters were computed from the histogram data rather than from the fits.

describes the increased effective viscosity felt by particles confined near the sample cell walls. We use viscosity values corrected for such wall-drag when applying eq 5 during data analysis. Although adequate theory,<sup>35</sup> validated by experiments,<sup>36–38</sup> currently exists to describe wall-drag effects in the diffusion of confined spherical particles, no comparable treatments are yet available for rod-shaped particles. In our data analysis we apply a constant wall-drag correction factor for nanotubes of all lengths, even though the use of an effective viscosity has been experimentally confirmed only for rigid rods that have lengths greater than  $1 \mu\text{m}$ .<sup>39,40</sup> If wall-drag effects were reduced or absent for shorter SWCNTs, then their deduced lengths would be severely underestimated in our analysis. However, Figures 2 and 4 illustrate that applying a length-independent SWCNT wall-drag correction gives results consistent with conventional AFM analysis. We also note that other workers have reported increased drag on particles that are much smaller than the dimensions of confinement.<sup>36</sup> Further LAND studies of SWCNT samples with narrower length distributions may provide new insights into the motions of high aspect-ratio rigid rods in confined liquid environments.

## CONCLUSIONS

We have demonstrated a practical new method for measuring length distributions of suspended SWCNTs. Near-IR fluorescence videomicroscopy is used to

simultaneously observe dozens of individual nanotubes and to record their Brownian motions in fluid solutions. Customized image analysis software automatically extracts the trajectories of the observed nanotubes, evaluates their individual diffusion coefficients, computes the corresponding lengths, and compiles the results into a histogram showing the sample's length distribution. The new method has been validated by comparison with distributions found by conventional AFM analysis.

A limitation of this LAND method is that it can be used only with underivatized semiconducting SWCNTs that emit at wavelengths detectable by the available camera. Also, to avoid undercounting short nanotubes, a single  $(n,m)$  species should be selected through optical filtering of the emission and resonant excitation at a relatively high intensity. Although we have used an InGaAs imager in the present study, it is also possible to implement the LAND method using a more common red-sensitive Si camera if small diameter SWCNTs such as (8,3) or (6,5) are selected for observation. An advantage of the LAND method over AFM is its capability of providing a length histogram of  $\sim 800$  nanotubes in approximately 2 h, with a high level of automation and lower operator effort. Less detailed analyses to find mean lengths rather than full distributions can be performed in a fraction of that time. In addition, LAND is less susceptible to impurity and bundling artifacts than AFM or light scattering methods. The near-IR fluorescence images used for LAND analysis

are also useful for revealing the emissive loose aggregates of SWCNTs that indicate early stages of sample agglomeration. We expect that diffusional

length analysis will prove a valuable tool for characterizing SWCNT samples and aiding the development of new length sorting methods.

## EXPERIMENTAL METHODS

**Sample Preparation and Solution Viscosity.** Approximately 5 mg of raw HiPco nanotubes (Rice University reactor, batch HPR 188.4) were suspended in 10 mL of 2% aqueous sodium cholate using 1 h of bath sonication (Sharpertek Stamina XP) followed by 30 min of tip sonication (Misonix Microson XL) at a power of 7 W. The suspension was centrifuged at 13300g for 1 h to remove nanotube bundles and residual iron catalyst. The supernatant was then diluted to an absorbance of  $\sim 10$  per cm at 984 nm and used as the starting material for nonlinear density gradient ultracentrifugation processing, following the method of Ghosh *et al.*<sup>33</sup> This provided SWCNT samples highly enriched in the (6,5) species.

Length fractionated samples were prepared through a technique based on the molecular crowding induced clustering of DNA-wrapped SWCNTs.<sup>34</sup> SWCNTs (grade S-P95-02-Dry, batch Du1-A001 CoMoCat) were purchased from Southwest Nanotechnologies (Norman, OK), and DNA oligomers were purchased from IDT-DNA (Coralville, IA). To 1 mg of SWCNTs were added 120  $\mu$ L of 10 mg/mL (GT)<sub>20</sub> oligomer in DI water, 800  $\mu$ L of DI water, and 100  $\mu$ L of 20 $\times$  SSC buffer (300 mmol/L sodium citrate, 3 mol/L sodium chloride). The mixture was sonicated for 60 min at 6 W. The resulting suspension was centrifuged at 18  $^{\circ}$ C and 17000g in 100  $\mu$ L aliquots for 90 min. This DNA-SWCNT dispersion was diluted with DI water to a final concentration of 80  $\mu$ g/mL SWCNT. A 5 M NaCl solution was added to a final concentration of 0.500 M, and 50% stock 6 kDa PEG solution was added to the desired final concentration for the first precipitation step. This mixture was incubated overnight at 4  $^{\circ}$ C. After incubation, the mixture was centrifuged at 18  $^{\circ}$ C and 8000g for 10 min. The supernatant was removed and more PEG was added to the supernatant to increase the concentration for the next precipitation step. The pellet was redispersed, by pipetting several times, in 0.100 M NaCl. Additional DNA was added to a final concentration of 100  $\mu$ g/mL for improved stability. The PEG concentrations used (fraction numbers) were: 1.4% (F8), 2% (F7), 2.6% (F6), 3.2% (F5), 4% (F4), 4.8% (F3), 5.6% (F2), and 6.4% (F1).

Shorter nanotubes are difficult to track in fluorescence videomicroscopy because they emit less light and diffuse quickly, spreading their emission over several pixels during each image exposure. To avoid this problem, we increased the solution viscosity to 30 mPa-s by diluting 1  $\mu$ L of SWCNT suspension with 500  $\mu$ L of a 60% sorbitol/1% deoxycholate solution. The viscosity of the sorbitol solution was measured with a Cannon–Fenske routine viscometer (size 150) and correlated with refractive index values.

**Fabrication of Glass Microwells.** A 5  $\times$  5 array of circular microwells (1 mm in diameter) was wet-etched into a glass microscope slide using a buffered oxide etch (BOE) comprising a 6:1 volume ratio of 40% aqueous NH<sub>4</sub>F to 49% HF. Etching time was 25 s at room temperature. To protect the surrounding substrate from the etchant, Microposit S1813 positive photoresist was spin-coated onto the glass slide at 3000 rpm to create an approximate 2  $\mu$ m thick mask. A SUSS MicroTec MJB4 mask aligner patterned the microwell grid onto the mask using 365 nm UV light at 5 W. Exposure time was 5 s and Microposit MF-319 was used as the developer. The mean well depth was measured to be 1.60  $\pm$  0.03  $\mu$ m using a Veeco Dektak 6 M profilometer. This depth corresponds to the approximate depth of field of our microscope objective.

**Sample Loading.** A 1  $\mu$ L drop of SWCNT suspension was placed in the center of the glass slide containing the microwell array. A coverslip was then applied with heavy manual pressure to force the SWCNT sample into the microwells, and the edges of the coverslip were immediately sealed with vacuum grease to prevent evaporation and convection. In this process, a thin liquid layer remained between the outer surfaces of the glass slide and coverslip, increasing the effective depth of each well.

The difference between the concentration of SWCNTs inside and outside the wells let us estimate that this extra depth was typically less than 200 nm. This estimate was confirmed by observing that the vast majority of SWCNTs located inside the microwells were unable to diffuse out.

**Near-IR Videomicroscopy.** As described previously,<sup>17</sup> near-infrared images of diffusing (6,5) SWCNTs were acquired using an inverted Nikon TE-2000U microscope equipped with a Nikon PlanApo 60 $\times$ /1.4 NA oil immersion objective lens. A dichroic beamsplitter and 946 nm long-pass filter were used to select the desired near-IR emission, which was detected with a liquid nitrogen-cooled InGaAs camera (Roper Scientific OMA-V 2D). We used 840 nm light from a continuous wave Ti:sapphire laser (Del Mar Photonics) to excite the broad E<sub>11</sub> vibronic sideband transition of (6,5) SWCNTs. The use of this excitation wavelength gives reduced background emission from glass trace impurities, especially Nd<sup>3+</sup> ions. The maximum excitation intensity at the sample was  $\sim 1.4$  kW/cm<sup>2</sup>. Excitation light was converted to circular polarization using a  $\lambda/4$  retardation plate to minimize fluorescence blinking caused by nanotube rotation. When analyzing the length fractionated CoMoCAT samples, a 1000 nm short-pass filter was placed in the emission path to spectrally select for (6,5) SWCNT emission. Image sequences contained 1001 frames with a 150 ms exposure time per frame. Each sample analysis was based on a set of 20 such sequences measured from different positions in the sample.

**Atomic Force Microscopy.** AFM samples of the (6,5) enriched DGU suspension were prepared by spin coating small drops of the SWCNT sample onto a silicon wafer. The wafer was then washed with water to remove excess surfactant. Images were acquired using a Veeco Multimode 3A atomic force microscope. For the length fractionated samples prepared by PEG precipitation, samples were deposited on freshly cleaved mica. The DNA-SWCNT sample was diluted to a final concentration of  $\sim 1$   $\mu$ g/mL into 15 mM KCl. Since KCl neutralizes the charge on Muscovite mica, deposition was rapid and a sufficient number of CNTs were observed after 2 to 15 min of incubation. A model MFP-3D AFM (Asylum Research, Santa Barbara, CA) was used for observations. We measured  $\sim 800$  SWCNTs to construct each histogram.

Certain commercial equipment, instruments, or materials are identified in this paper in order to specify the experimental procedure adequately. Such identification is not intended to imply recommendation or endorsement by the National Institute of Standards and Technology, nor is it intended to imply that the materials or equipment identified are necessarily the best available for the purpose. Unless noted otherwise, all reagents were obtained from standard sources.

**Conflict of Interest:** The authors declare no competing financial interest.

**Acknowledgment.** This work was supported by the Welch Foundation (Grant C-0807) and the National Science Foundation (Grant CHE-1112374). We thank G. Canning for providing (6,5) enriched SWCNT samples and for useful discussions, D. Tsybolski for consultations on image analysis, and T. Gilheart for helpful suggestions in the fabrication of the glass microwells.

**Supporting Information Available:** Empirical formulas representing uncertainties in MSD slopes as a function of localization error and number of fitting points, and data related to convective drift effects. This material is available free of charge via the Internet at <http://pubs.acs.org>.

## REFERENCES AND NOTES

1. Becker, M. L.; Fagan, J. A.; Gallant, N. D.; Bauer, B. J.; Bajpai, V.; Hobbie, E. K.; Lacerda, S. H.; Migler, K. B.; Jakupciak, J. P. Length-Dependent Uptake of DNA-Wrapped Single-Walled Carbon Nanotubes. *Adv. Mater.* **2007**, *19*, 939–945.

2. Jin, H.; Heller, D. A.; Sharma, R.; Strano, M. S. Size-Dependent Cellular Uptake and Expulsion of Single-Walled Carbon Nanotubes: Single Particle Tracking and a Generic Uptake Model for Nanoparticles. *ACS Nano* **2009**, *3*, 149–158.
3. Avouris, P.; Chen, Z.; Perebeinos, V. Carbon-Based Electronics. *Nat. Nanotechnol.* **2007**, *2*, 605–615.
4. Hecht, D.; Hu, L.; Gruner, G. Conductivity Scaling with Bundle Length and Diameter in Single Walled Carbon Nanotube Networks. *Appl. Phys. Lett.* **2006**, *89*, 133112.
5. Coleman, J. N.; Khan, U.; Blau, W. J.; Gun'ko, Y. K. Small but Strong: A Review of the Mechanical Properties of Carbon Nanotube-Polymer Composites. *Carbon* **2006**, *44*, 1624–1652.
6. Laborde-Lahoz, P.; Maser, W.; Martinez, T.; Benito, A.; Seeger, T.; Cano, P.; de Villoria, R. G.; Miravete, A. Mechanical Characterization of Carbon Nanotube Composite Materials. *Mech. Adv. Mater. Struct.* **2005**, *12*, 13–19.
7. Ziegler, K. J.; Rauwald, U.; Gu, Z. N.; Liang, F.; Billups, W. E.; Hauge, R. H.; Smalley, R. E. Statistically Accurate Length Measurements of Single-Walled Carbon Nanotubes. *J. Nanosci. Nanotechnol.* **2007**, *7*, 2917–2921.
8. Wang, S. R.; Liang, Z. Y.; Wang, B.; Zhang, C. Statistical Characterization of Single-Wall Carbon Nanotube Length Distribution. *Nanotechnology* **2006**, *17*, 634–639.
9. Badaire, S.; Poulin, P.; Maugey, M.; Zakri, C. *In Situ* Measurements of Nanotube Dimensions in Suspensions by Depolarized Dynamic Light Scattering. *Langmuir* **2004**, *20*, 10367–10370.
10. Lee, J. Y.; Kim, J. S.; An, K. H.; Lee, K.; Kim, D. Y.; Bae, D. J.; Lee, Y. H. Electrophoretic and Dynamic Light Scattering in Evaluating Dispersion and Size Distribution of Single-Walled Carbon Nanotubes. *J. Nanosci. Nanotechnol.* **2005**, *5*, 1045–1049.
11. Bauer, B. J.; Fagan, J. A.; Hobbie, E. K.; Chun, J.; Bajpai, V. Chromatographic Fractionation of SWNT/DNA Dispersions with on-Line Multiangle Light Scattering. *J. Phys. Chem. C* **2008**, *112*, 1842–1850.
12. Chun, J.; Fagan, J. A.; Hobbie, E. K.; Bauer, B. J. Size Separation of Single-Wall Carbon Nanotubes by Flow-Field Flow Fractionation. *Anal. Chem.* **2008**, *80*, 2514–2523.
13. Shetty, A.; Wilkins, G. M. H.; Nanda, J.; Solomon, M. J. Multiangle Depolarized Dynamic Light Scattering of Short Functionalized Single-Walled Carbon Nanotubes. *J. Phys. Chem.* **2009**, *113*, 7129–7133.
14. Casey, J. P.; Bachilo, S. M.; Moran, C. H.; Weisman, R. B. Chirality-Resolved Length Analysis of Single-Walled Carbon Nanotube Samples through Shear-Aligned Photoluminescence Anisotropy. *ACS Nano* **2008**, *2*, 1738–1746.
15. Cherukuri, T. K.; Tsybolski, D. A.; Weisman, R. B. Length- and Defect-Dependent Fluorescence Efficiencies of Individual Single-Walled Carbon Nanotubes. *ACS Nano* **2012**, *6*, 843–850.
16. Tsybolski, D. A.; Bachilo, S. M.; Kolomeisky, A. B.; Weisman, R. B. Translational and Rotational Dynamics of Individual Single-Walled Carbon Nanotubes in Aqueous Suspension. *ACS Nano* **2008**, *2*, 1770–1776.
17. Tsybolski, D. A.; Bachilo, S. M.; Weisman, R. B. Versatile Visualization of Individual Single-Walled Carbon Nanotubes with Near-Infrared Fluorescence Microscopy. *Nano Lett.* **2005**, *5*, 975–979.
18. Heller, D. A.; Baik, S.; Eurell, T. E.; Strano, M. S. Single-Walled Carbon Nanotube Spectroscopy in Live Cells: Towards Long-Term Labels and Optical Sensors. *Adv. Mater.* **2005**, *17*, 2793–2799.
19. Cognet, L.; Tsybolski, D.; Rocha, J.-D. R.; Doyle, C. D.; Tour, J. M.; Weisman, R. B. Stepwise Quenching of Exciton Fluorescence in Carbon Nanotubes by Single-Molecule Reactions. *Science* **2007**, *316*, 1465–1468.
20. Reuel, N. F.; Dupont, A.; Thouvenin, O.; Lamb, D. C.; Strano, M. S. Three-Dimensional Tracking of Carbon Nanotubes within Living Cells. *ACS Nano* **2012**, *6*, 5420–5428.
21. Qian, H.; Sheetz, M. P.; Elson, E. L. Single Particle Tracking: Analysis of Diffusion and Flow in Two-Dimensional Systems. *Biophys. J.* **1991**, *60*, 910–921.
22. Saxton, M. J. Single-Particle Tracking: The Distribution of Diffusion Coefficients. *Biophys. J.* **1997**, *72*, 1744–1753.
23. Thompson, R. E.; Larson, D. R.; Webb, W. W. Precise Nanometer Localization Analysis for Individual Fluorescent Probes. *Biophys. J.* **2002**, *82*, 2775–2783.
24. Ober, R. J.; Ram, S.; Ward, E. S. Localization Accuracy in Single-Molecule Microscopy. *Biophys. J.* **2004**, *86*, 1185–1200.
25. Savin, T.; Doyle, P. S. Static and Dynamic Errors in Particle Tracking Microrheology. *Biophys. J.* **2005**, *88*, 623–638.
26. Montiel, D.; Cang, H.; Yang, H. Quantitative Characterization of Changes in Dynamical Behavior for Single-Particle Tracking. *J. Phys. Chem.* **2006**, *110*, 19763–19770.
27. Michalet, X. Mean Square Displacement Analysis of Single-Particle Trajectories with Localization Error: Brownian Motion in an Isotropic Medium. *Phys. Rev. E* **2010**, *82*, 041914–1–041914–13.
28. Berglund, A. J. Statistics of Camera-Based Single-Particle Tracking. *Phys. Rev. E* **2010**, *82*, 011917–1–011917–8.
29. Duggal, R.; Pasquali, M. Dynamics of Individual Single-Walled Carbon Nanotubes in Water by Real-Time Visualization. *Phys. Rev. Lett.* **2006**, *96*, 246104–1–246104–4.
30. Fakhri, N.; Tsybolski, D. A.; Cognet, L.; Weisman, R. B.; Pasquali, M. Diameter-Dependent Bending Dynamics of Single-Walled Carbon Nanotubes in Liquids. *Proc. Natl. Acad. Sci. U.S.A.* **2009**, *106*, 14219–14223.
31. Aragon, S. R.; Flamik, D. High Precision Transport Properties of Cylinders by the Boundary Element Method. *Macromolecules* **2009**, *42*, 6290–6299.
32. Arnold, M. S.; Suntivich, J.; Stupp, S. I.; Hersam, M. C. Hydrodynamic Characterization of Surfactant Encapsulated Carbon Nanotubes Using an Analytical Ultracentrifuge. *ACS Nano* **2008**, *2*, 2291–2300.
33. Ghosh, S.; Bachilo, S. M.; Weisman, R. B. Advanced Sorting of Single-Walled Carbon Nanotubes by Nonlinear Density-Gradient Ultracentrifugation. *Nat. Nanotechnol.* **2010**, *5*, 443–450.
34. Khripin, C. Y.; Arnold-Medabalimi, N.; Zheng, M. Molecular-Crowding-Induced Clustering of DNA-Wrapped Carbon Nanotubes for Facile Length Fractionation. *ACS Nano* **2011**, *5*, 8258–8266.
35. Brenner, H. The Slow Motion of a Sphere Through a Viscous Fluid Towards a Plane Surface. *Chem. Eng. Sci.* **1961**, *16*, 242–251.
36. Lin, B.; Yu, J.; Rice, S. A. Direct Measurements of Constrained Brownian Motion of an Isolated Sphere Between Two Walls. *Phys. Rev. E* **2000**, *62*, 3909–3919.
37. Carbajal-Tinoco, M. D.; Lopez-Fernandez, R.; Arauz-Lara, J. L. Asymmetry in Colloidal Diffusion Near a Rigid Wall. *Phys. Rev. Lett.* **2007**, *99*, 138303–1–138303–4.
38. Eral, H. B.; Oh, J. M.; Van Den Ende, D.; Mugele, F.; Duits, M. H. G. Anisotropic and Hindered Diffusion of Colloidal Particles in a Closed Cylinder. *Langmuir* **2010**, *26*, 16722–16729.
39. Li, G.; Tang, J. X. Diffusion of Actin Filaments within a Thin Layer between Two Walls. *Phys. Rev. E* **2004**, *69*, 061921–1–061921–5.
40. Marshall, B. D.; Davis, V. A.; Lee, D. C.; Korgel, B. A. Rotational and Translational Diffusivities of Germanium Nanowires. *Rheol. Acta* **2009**, *48*, 589–596.